Advanced Photonics Research

ADVANCED PHOTONICS RESEARCH Open Access

www.adpr-journal.com

RESEARCH ARTICLE OPEN ACCESS

Effect of 40 Hz Light Stimulation on Calcium Dynamics of Astrocytes

Aikaterini Konstantoulaki[1,2] | Maibritt Horning[3,4] | Tjalfe Egholm Rude[4,5] | Roberta Fabbri[1] | Chiara Lazzarini[1] | Giorgia Conte[1] | Andrea Candini[1] | Marco Caprini[6,7] | Marcus Schultz Carstensen[4] | Valentina Benfenati[1]

[1]Institute for Organic Synthesis and Photoreactivity, National Research Council, Bologna, Italy | [2]Department of Chemistry, University of Bologna, Bologna, Italy | [3]Department of Clinical Medicine, Faculty of Health and Medical Sciences, University of Copenhagen, Copenhagen, Denmark | [4]OptoCeutics ApS, Copenhagen, Denmark | [5]Technical University of Denmark, Lyngby, Denmark | [6]Department of Pharmacy and Biotechnology, University of Bologna, Bologna, Italy | [7]IRCCS, Istituto delle Scienze Neurologiche di Bologna, Bologna, Italy

Correspondence: Marcus Schultz Carstensen (msc@optoceutics.com) | Valentina Benfenati (valentina.benfenati@cnr.it)

Received: 18 August 2025 | **Revised:** 28 January 2026 | **Accepted:** 25 February 2026

Keywords: 40 Hz invisible spectral flicker (ISF) | astrocyte calcium signaling | LED visible photostimulation

ABSTRACT

Astrocytes are glial cells with intracellular calcium dynamics essential for brain homeostasis, synaptic modulation, and cognition and altered in neuropathology and neuroinflammation. Growing evidence indicates these calcium signals can be triggered by chemophysical stimuli. Photonic, label free optical stimulation could provide unique opportunities to study astrocytic calcium signaling in physiological and pathological conditions and responses to external cues. This study describes the effects of visible LED light technology, called 40 Hz invisible spectral flicker (ISF), on calcium dynamics in primary rat cortical astrocytes. We demonstrate that ISF and continuous visible light (CL, used as control) can efficiently trigger calcium dynamics in astrocyte, through recruiting distinct molecular pathways. Specifically, extracellular calcium influx is essential for the response to 40 Hz ISF stimulation to occur but not to CL. In addition,the channels TRPV4 and TRPA1, as well as IP_3Rs and ryanodine receptors pathways, are differentially implicated in the observed effects in response to ISF and CL. These findings respond to the need for novel methods to trigger calcium signaling in astrocytes, showing that ISF visible, nonlaser light is an effective approach with potential modulation capability simply varying light stimulation frequency.

1 | Introduction

Neurocentric research has long overlooked glial cells, but they are now recognized as key regulators of neuronal activity and vital contributors to synapse formation, neural repair, and brain function [1–3]. Astrocytes support brain homeostasis, mediate intercellular communication, and play essential roles in cognitive processes and cerebrovascular regulation [4, 5]. Emerging evidence underscores the active role of astrocytes in regulating neural oscillations through bidirectional communication with neurons [6, 7]. Astrocytes respond to neurotransmitters with calcium signaling and release gliotransmitters, modulating both excitatory and inhibitory synaptic activity [8, 9].

Among the various dynamics that underpin the physiological roles of astrocytes, an intracellular rise in Ca^{2+} signals is observed in response to changes in extracellular and intracellular homeostatic cues, including mechanical, chemophysical, and biological alterations occurring within both physiological and pathological ranges [10]. $[Ca^{2+}]$ may derive from the extracellular space via channels that include Transient Receptor Potential Ankyrin 1 (TRPA1) and Transient Receptor Potential Vanilloid 4 (TRPV4) [11–14] or from intracellular stores which include the

Aikaterini Konstantoulaki and Maibritt Horning contributed equally to this work.

Endoplasmic Reticulum and the mitochondria [15]. Alterations in astrocytic calcium dynamics have been linked to neuroinflammatory responses, impaired neuronal function, and broader network dysregulation [16, 17].

Given the importance of diverse astroglial calcium signaling in brain physiology and pathology, recent studies have begun to employ label-free biophotonic tools that provide fast, efficient, and precise methods for controlling calcium signaling in astrocytes [18, 19]. Studies have shown that astrocytes' calcium signaling can be elicited by laser light at different frequencies and power density [20–23]. Calcium signaling through TRPV4, TRPA1, and IP_3, as well as water transport, could be triggered by 1874 nm single-pulse laser light [21]. Notably, the use of 100 times less amount of laser light and UV frequency induces exclusively intracellular calcium release and not extracellular calcium influx [22, 23]. Although the use of laser light to excite, modulate, or inhibit astrocytic calcium signaling has been reported, and some mechanistic insights underlying these effects have been described, evidence regarding the impact of noncoherent visible light delivered by light-emitting diodes (LEDs) on astrocytes remains limited. However, a substantial body of literature indicates that, in addition to classical photoreceptors, cells possess various intracellular organelles, such as mitochondria, as well as molecular components, including reactive oxygen species, water, and membrane lipids, that are capable of absorbing light energy and initiating signaling cascades without requiring photochemical conversion or thermal effects [18, 24–27]. Here, we sought to address this gap in knowledge by investigating the effects of 40 Hz visible light stimulation on astroglial calcium dynamics in vitro, using invisible spectral flicker (ISF) technology [28]. This approach enabled us to examine the impact of LED-based visible light on astrocytes while minimizing luminance flicker and its potential confounding effects on cellular responses. ISF alternates between two spectrally distinct color profiles of visible light, generating a flicker at a defined frequency (e.g., 40 Hz). The two-color profiles are matched in color properties and luminance, creating a flicker that is nearly imperceptible by the human eye, in contrast to conventional stroboscopic or luminance-based flicker [29].

In vivo evidence indicated that 40 Hz light stimulation is linked to changes in astroglial glymphatic function, a clearance homeostatic process that is regulated by intracellular calcium dynamics [30–33], yet the cellular mechanisms remain to be defined. In this regard, a recent study suggests that *in vitro*, astroglial purinergic signaling is involved in the glymphatic response of astrocytes to 40 Hz light stimulation. However, the effects of 40 Hz visible LED light on astroglial calcium dynamics have never been reported.

By combining ISF stimulation with Fluo-4-based calcium imaging and a comprehensive pharmacological characterization, we demonstrate that visible light delivered at different stimulation frequencies, while maintaining the same power density, selectively induces distinct Ca^{2+} dynamics and engages downstream signaling pathways, including G-protein-coupled receptors (GPCRs). Collectively, our results show that ISF light is a valuable tool for studying and modulating astroglial calcium signaling and related intracellular pathways. The herein presented findings set the basis for future studies aiming to unveil cellular mechanisms beyond 40 Hz light stimulation on neural circuitry.

2 | Materials and Methods

2.1 | Rat Cortical Astrocyte Culture Preparation, Maintenance, and Plating

Primary cultures of cortical astrocytes from newborn Sprague–Dawley rats were prepared as previously described [34], following the Italian regulations on the protection of laboratory animals, with the approval of bioethical committees of the University of Bologna and of the Ministry of Health (ID 1268, code number 2DBFE.N.HTT) and under the supervision of the veterinary commission for animal care and comfort at the University of Bologna. In brief, after removal of the meninges, the cerebral cortices of 1- to 2-day-old rats (P0–P2) were mechanically dissociated and placed in cell culture flasks containing DMEM–GlutaMAX medium supplemented with 15% fetal bovine serum, 100 U/mL penicillin, and 100 mg/mL streptomycin (all purchased from Gibco–Invitrogen). The culture flasks were maintained in a humidified incubator at 37°C and 5% CO_2 for 3 to 4 weeks. The culture medium was replaced every 2 days, and before medium change, flasks were gently shaken to detach microglial cells seeded on the astrocytic monolayer. After reaching confluence of ~80%, the cells were enzymatically dispersed with 0.25% Trypsin/EDTA (Thermo Fisher Scientific) and then seeded on poly-D-lysine (PDL)-coated glass coverslips at a density of 16.000 cells/cm^2. Cells were maintained in culture medium containing 10% FBS. Experiments of calcium microfluorometry were performed after 5 days *in vitro*.

2.2 | Light Stimulation of Primary Astrocytes

To investigate the effect of 40 Hz ISF on astrocytic calcium dynamics, a customized version of the OptoCeutics Light Therapy System (LTS; OptoCeutics ApS, Copenhagen, Denmark), fabricated specifically for *in vitro* experiments, was used. The system consists of a control board incorporating a printed circuit board (PCB) connected to an LED board comprising six LEDs. The device is controlled using a custom Python script via a UART data connection to an experimental computer. The LED plate is encapsulated by a custom 3D-printed adapter designed to couple the light source to a 600-µm diameter optical fiber (Avantes). The adapter ensures minimal light loss and preserves the integrity of the light beam during transmission. At both ends of the fiber, collimating lenses (Avantes) were affixed to convert the light emitted from the LED source into a parallel (collimated) beam, ensuring uniform illumination of the cell culture.

Two light stimulation paradigms were employed: continuous light (CL) and ISF. CL is generated by simultaneous color mixing of 4 LEDs (blue, cyan, red, and lime), producing a white light with a 100% duty cycle (Figure 1B). ISF is generated by alternating

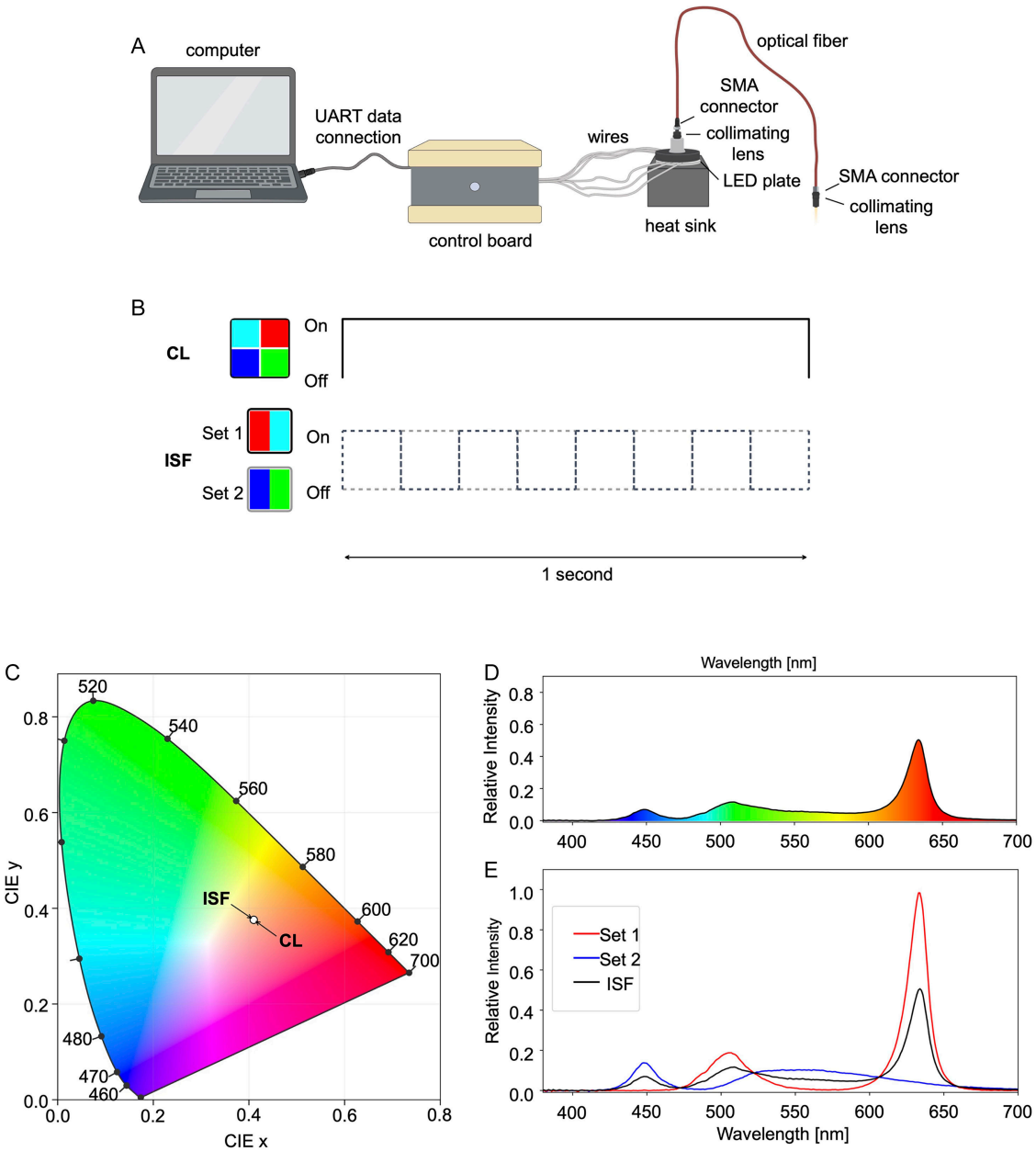

FIGURE 1 | Light stimulation delivery system and light properties. (A) 40 Hz ISF was delivered by a customized version of OptoCeutic's Light Therapy System (LTS; OptoCeutics ApS, Copenhagen, Denmark). (B) Color profile of ISF and CL light depicted in the CIE 1931 chromatic diagram. ISF and CL light settings are matched at the same intensity (1.3 mW/cm^2) and color temperature (3,191 K; chromaticity coordinates $(x, y) = (0.410, 0.376)$, indicated by a white dot). (C) Wavelength spectra of both ISF and CL. (D) Spectral composition of ISF light showing set 1 and set 2 spectra. (E) Comparison of CL and ISF light cycles depicted for 1 s. CL utilizes all four colors when on; ISF alternates between two spectral sets at 40 Hz; as there are no dark intervals between sets, a 100% duty cycle is maintained, ensuring equivalent fluence delivery. Created with PowerPoint (Microsoft), BioRender, and Python.

between two sets of LEDs (set 1: red, cyan; set 2: blue, lime) at 40 Hz, with each set comprising different spectral components (Figure 1E).

Because spectral alternation occurred without dark intervals, ISF maintains a 100% duty cycle, resulting in continuous light delivery rather than pulsed or stroboscopic illumination (Figure 1B). CL and ISF are matched in brightness (1.3 mW/cm^2 at 2 cm distance) and color temperature (3,191 K, with chromaticity coordinates of $(x, y) = (0.410, 0.376)$) (Figure 1C), resulting in an equivalent time-averaged emission spectrum (Figure 1D). The total fluence delivered was identical for both ISF and CL conditions (0.0065 J/cm^2; calculated as 1.3 mW/cm^2 × 5 s). Irradiance was measured using an optical power meter (Photodiode Power Sensor: S130C; Meter Console: PM400; Thorlabs). Importantly, ISF does not involve pulsed or stroboscopic light; rather, it utilizes continuous illumination with time-alternating spectral compositions at 40 Hz (Figure 1D,E). Two distinct LED sets (set 1 and set 2), each comprising different spectral components, alternate at 40 Hz while maintaining constant perceived brightness and color temperature (Carstensen et al., 2020). This spectral switching produces a 100%

duty cycle, meaning light is delivered continuously without dark intervals (Figure 1B).

During calcium imaging and light stimulation, the optical fiber was positioned at 2 cm above the coverslips containing the plated astrocytes and oriented at an angle of 45° relative to the plane of the PDL-treated coverslips (Figure 2). The experimental design included three conditions: a no-stimulation baseline recording, a 40 Hz ISF condition, and a CL condition (Figure 2).

2.3 | Temperature Measurement and Calculation

The temperature of the saline solution contained in a petri dish was measured with a NiCr/NiAl K-type thermocouple (RS) for 10 min of ISF and CL stimulation and was found to be stable. Furthermore, several physical features of the setup indicate that localized microheating at the astrocyte monolayer is unlikely. The delivered optical power was very low (1.3 mW/cm^2 for 5 s; fluence = 0.0065 J/cm^2), and visible wavelengths (400–700 nm) are minimally absorbed by aqueous media, limiting photothermal conversion. The fiber-coupled LED delivery system, positioned at 2 cm and 45°, further disperses the beam and prevents conductive heat transfer from the light source. Even assuming complete absorption of the delivered fluence, the resulting temperature change would be below the resolution of microthermometry (<0.01°C) and far smaller than values known to influence astrocytic Ca^{2+} dynamics (typically >1°C–2°C). Calculations are reported in the Results section.

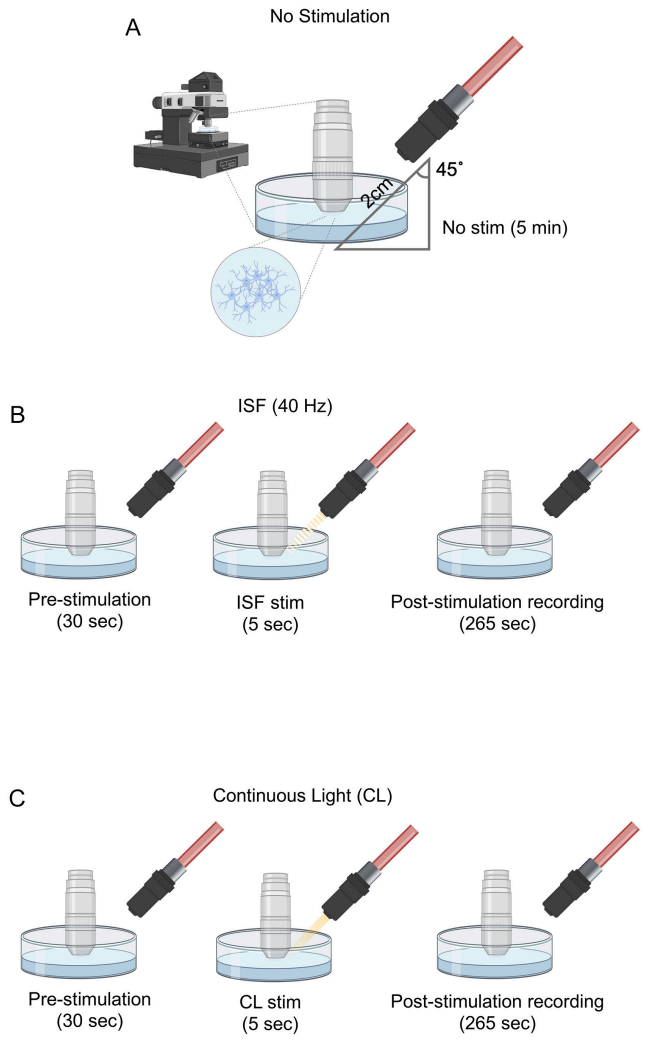

FIGURE 2 | Experimental setup for lightstimulation of astrocytes. Schematic representation of the calcium imaging and light stimulation apparatus. (A) A 600-μm diameter optical fiber (Avantes) with collimating lenses was positioned at 2 cm from the PDL-coated glass coverslips and oriented at 45° relative to the plane of the astrocyte culture. (B,C) Light stimulation (either 40 Hz ISF or continuous light; 1.3 mW/cm^2, 3,191 K) was delivered for 5 s while calcium dynamics were monitored using Fluo-4 AM fluorescence microscopy. Created with BioRender.

2.4 | Calcium Microfluorometry

Changes in the concentration of free intracellular calcium $[Ca^{2+}]_i$ were monitored by calcium microfluorometry using the single-wavelength fluorescent Ca^{2+} indicator Fluo-4 AM (Life Technologies), dissolved in control saline solution. Calcium imaging serves as a critical methodology for examining intracellular fluctuations of calcium ions. In this study, we employed the single-wavelength calcium indicator Fluo-4 AM to monitor these fluctuations in astrocytes *in vitro*. The measurements were conducted 5 days after the plating of 30,000 cells on 15-mm glass coverslips coated with PDL. Before imaging, cells were incubated in Fluo-4 AM (1 μM) for 30 min at room temperature. Fluorescence was excited using SPECTRA III light engine (Lumencor) at 475/28 nm and collected using a FITC/GFP filter at 525 nm. Calcium imaging was conducted using a fluorescence microscope (Olympus BX63) fitted with a 40× water objective. Time-lapse image acquisition and photostimulation were managed through Metamorph software (Molecular Devices). Camera exposure times were set to 150 ms, with an image sampling rate of 2 Hz. The data were obtained from independent experiments conducted in triplicate or more. Regions of interest (ROI) were defined within the cell soma. Fluorescence time series were manually extracted using Metamorph software (Molecular Devices, Sunnyvale, CA, USA). Each cell's raw fluorescence intensity was normalized to the mean raw intensity of the 20 frames preceding light stimulation, reported and analyzed as a fraction (ΔF_t/Ft_0). A cell was classified as responding when a 10% increase in normalized fluorescence was detected following light or stimulus exposure. Note that a transient light artifact is visible in the fluorescence traces during the 5-s stimulation period (dashed line in Figures 3–7). Importantly, the same transient was also detected in background regions lacking cells (and thus lacking intracellular Fluo-4). This artifact results from scattered stimulation light reaching the camera sensor and does not represent Ca^{2+}-dependent fluorescence.

2.5 | Chemicals and Solutions

The standard bath solution was composed of (mM) 140 NaCl, 4 KCl, 2 MgCl2, 2 $CaCl_2$, 10 HEPES, 5 glucose; pH was adjusted to 7.4 with NaOH 1 M; and osmolarity was adjusted

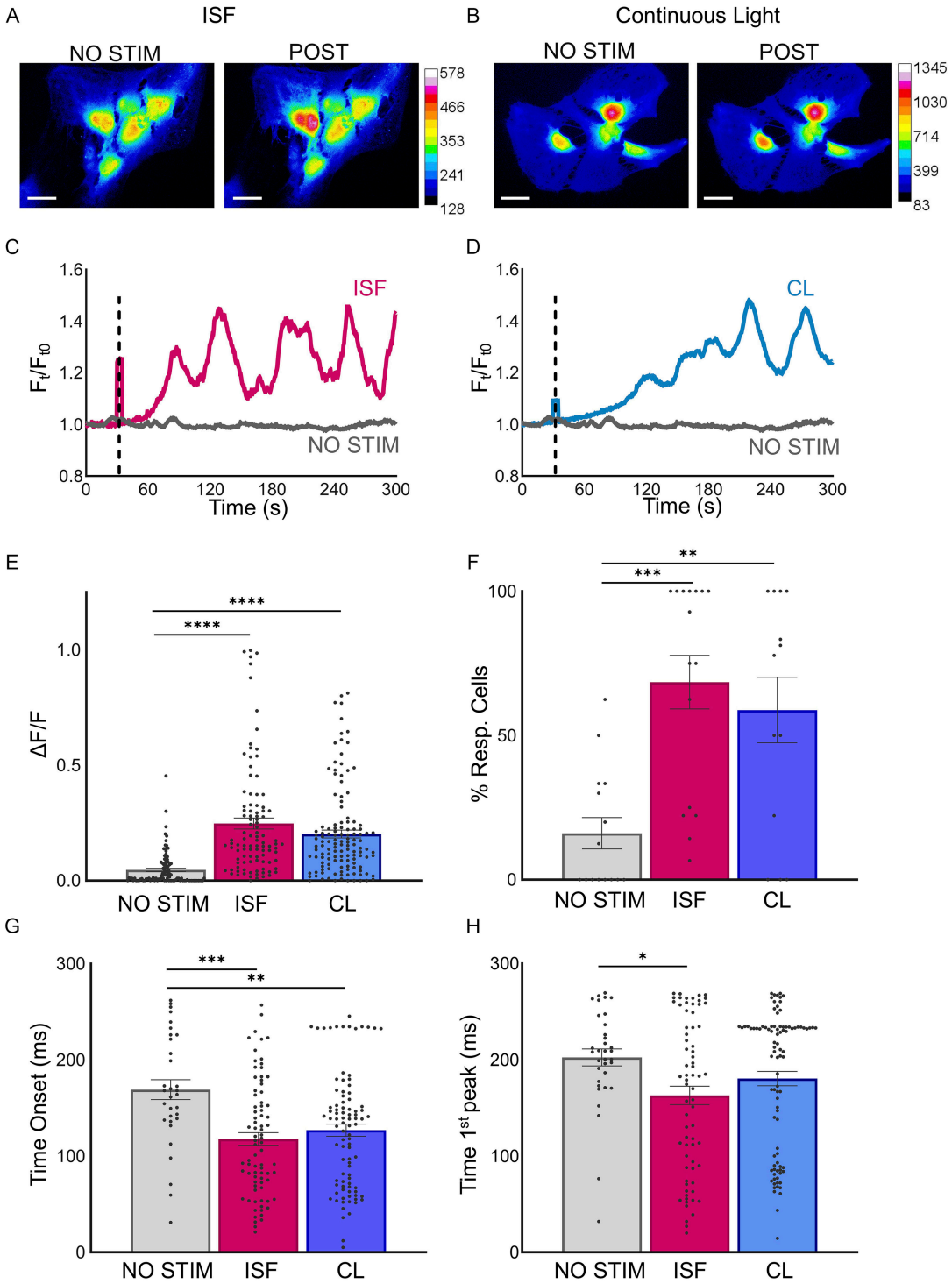

FIGURE 3 | ISF and continuous light induce different calcium dynamics on astrocytes in vitro. (A) Astrocytes on PDL-coated glass coverslips incubated in Fluo-4 pre- and post-40 Hz ISF stimulation and (B) pre- and post-CL stimulation (in pseudo color). (C) Representative calcium signaling traces of experiments performed using standard extracellular solution, no stimulation (gray), and after ISF stimulation (red). (D) Representative calcium signaling traces of experiments performed using standard extracellular solution, no stimulation (gray), and after CL stimulation (blue). (E–H) Histogram plots of measurements performed on astrocytes *in vitro*. All the results are expressed as mean ± SEM and statistical *p*-values. (E) Maximal fluorescence variation, (F) percentage of responding cells, (G) time onset (first fluorescence variation above the cutoff of the baseline–0.1, and (H) time to first peak. Scale bar = 50 μm. Data values corresponding to no stimulation are colored in gray, to ISF in cherry red, and to CL in blue. Asterisks denote significant differences: * ($p < 0.05$), ** ($p < 0.01$), *** ($p < 0.001$), **** ($p < 0.0001$). One-way ANOVA with Bonferroni correction. N = number of cells analyzed, n = number of experiments; For $\Delta F/F$:No stim $N = 106$, $n = 7$; ISF $N = 101$, $n = 7$; CL $N = 129$, $n = 7$. Sample sizes vary by metric; N (cells/ROIs) and n (experiments) for each panel are reported in Tables S1–S5, and *p*-values in Tables S6–S10.

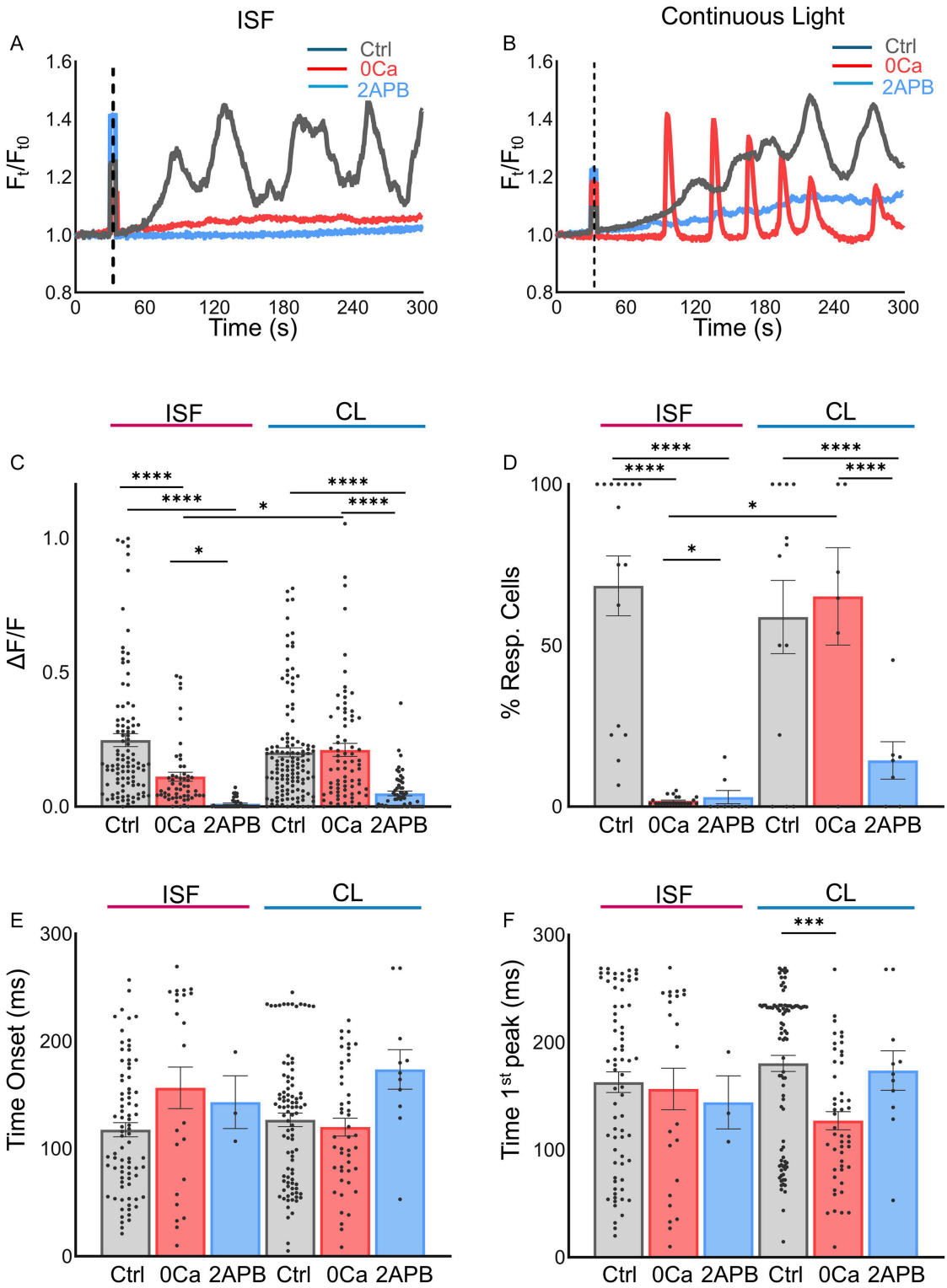

FIGURE 4 | Differential effects of calcium depletion and IP_3 receptor blockade on astrocyte calcium signaling. (A,B) Representative traces of astrocyte calcium signaling using standard extracellular solution, extracellular solution depleted of Ca^{2+} ($0[Ca^{2+}]_o$), and extracellular solution with 2-aminoethoxydiphenylborane (2-APB) at 100 μM after ISF (A) and continuous light stimulation (B). (C–F) Histogram plots of measurements performed on astrocytes in vitro. All the results are expressed as mean ± SEM and statistical *p*-values. (C) Maximal fluorescence variation, (D) percentage of responding cells, (E) time onset (first fluorescence variation above the cut-off of the baseline-0.1), and (F) time to the first peak. Data values corresponding to control are colored in gray, $0[Ca^{2+}]_o$ in red, and 2-APB in blue. Asterisks denote significant differences: * ($p < 0.05$), ** ($p < 0.01$), *** ($p < 0.001$), **** ($p < 0.0001$), one-way ANOVA with Bonferroni correction. For $\Delta F/F$:ISF control $N = 101$, $n = 7$; ISF $0[Ca^{2+}]_o$ $N = 55$, $n = 5$; ISF 2-APB, $N = 41$, $n = 4$; CL control $N = 129$, $n = 7$; CL $0[Ca^{2+}]_o$ $N = 75$, $n = 5$; CL 2-APB $N = 59$, $n = 4$. *N*, number of analyzed cells (regions of interest); *n*, number of experiments. Sample sizes vary by metric; *N* (cells/ROIs) and *n* (experiments) for each panel are reported in Tables S1–S5, and *p*-values in Tables S6–S10.

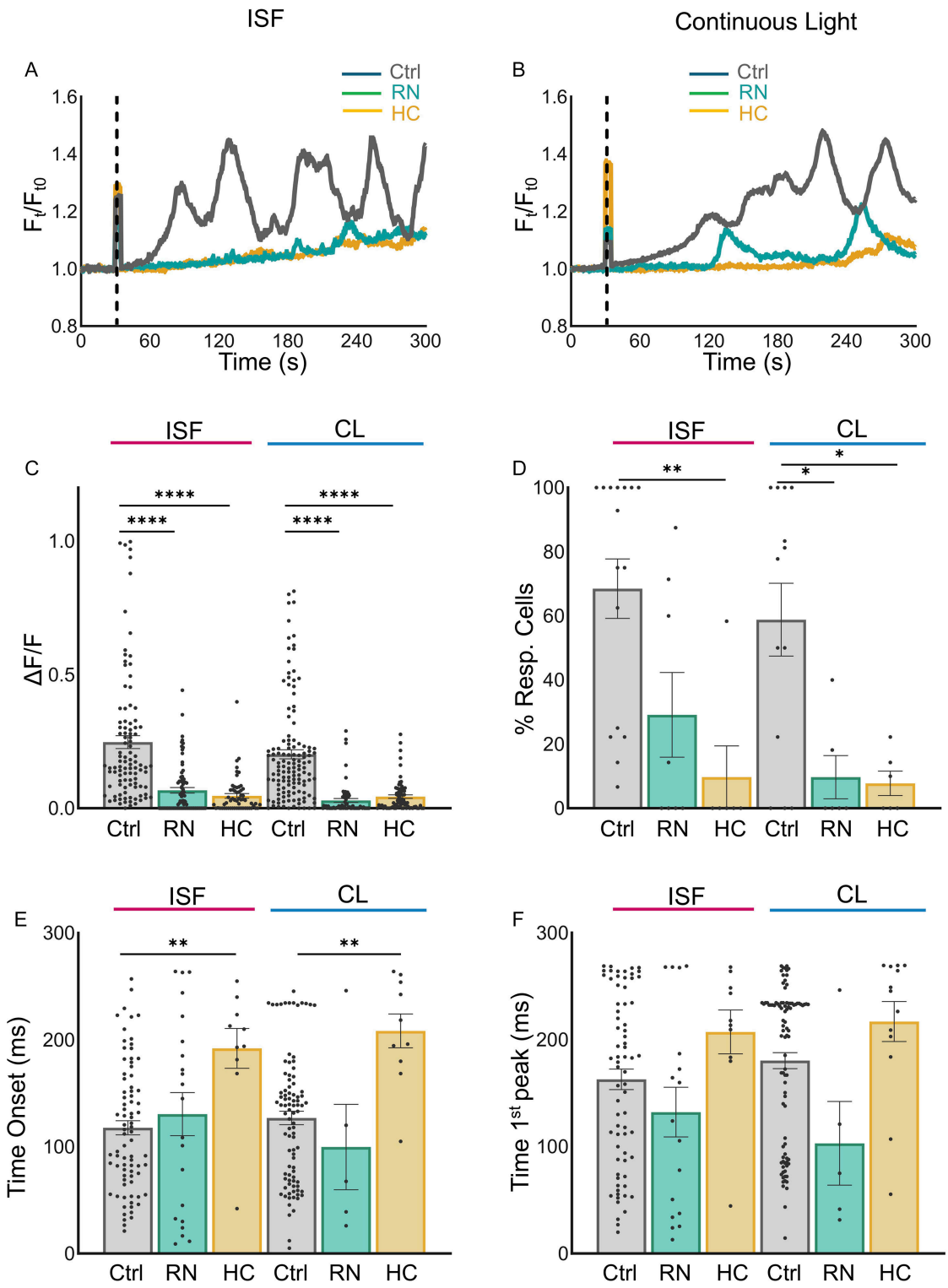

FIGURE 5 | TRPV4 and TRPA1 are involved in astrocytic calcium responses after ISF and CL stimulation. (A,B) Representative traces of astrocytes calcium signaling using TRPV4 inhibitor RN-1734 (10 μM) and (B) TRPA1 inhibitor HC-030031 (40 μM) after ISF (A) and continuous light stimulation (B). (C–F) Histogram plots of measurements performed on astrocytes in vitro corresponding to control are colored in gray, to RN-1734 (RN) in teal and HC-030031 (HC) in gold. All the results are expressed as mean ± SEM and statistical *p*-values. (C) Maximal fluorescence variation, (D) percentage of responding cells, (E) time onset (first fluorescence variation above the cutoff of the baseline-0.1), and (F) time to first peak. Asterisks denote significant difference: * ($p < 0.05$), ** ($p < 0.01$), *** ($p < 0.001$), **** ($p < 0.0001$). One-way ANOVA with Bonferroni correction. For $\Delta F/F$ (all cells, responding and not responding): ISF control $N = 101$, $n = 7$; ISF RN-1734 $N = 80$, $n = 4$; ISF HC-030031 $N = 58$, $n = 3$; CL control $N = 129$, $n = 7$; CL RN-1734 $N = 66$, $n = 4$; CL HC-030031 $N = 76$, $n = 3$. *N*, number of analyzed cells (regions of interest), *n*, number of experiments. Sample sizes vary by metric; N (cells/ROIs) and n (experiments) for each panel are reported in Tables S1–S5, and *p*-values in Tables S6–S10.

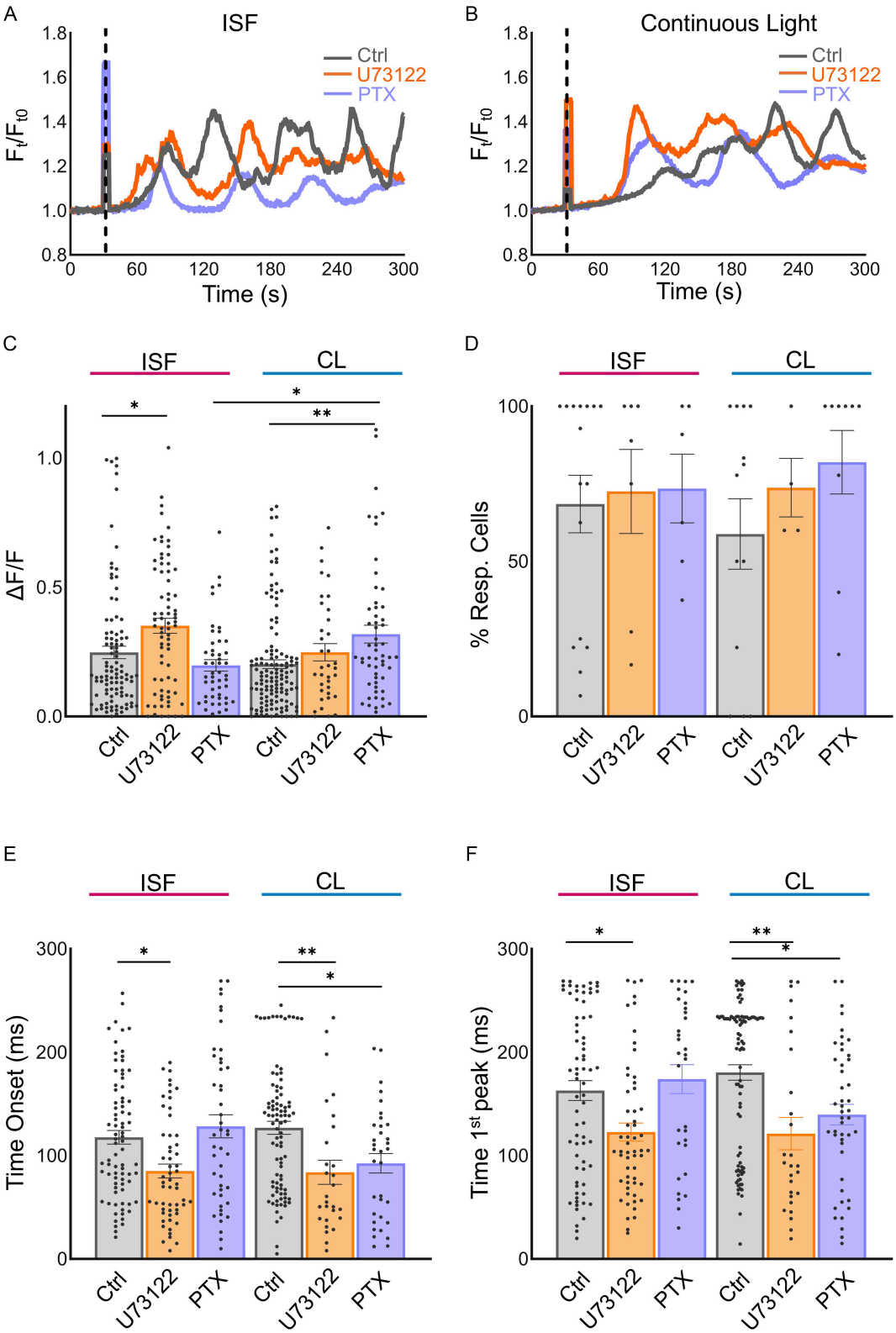

FIGURE 6 | Involvement of G_q–PLC–IP_3 and $G_{i/o}$ in astrocytic responses after ISF and CL stimulation. (A,B) Representative traces of astrocyte calcium signaling using G_q–PLC–IP_3 inhibitor U73122 (0.5 μM) and $G_{i/o}$ inhibitor pertussis toxin (PTX) (500 ng ml^{-1}) after ISF (A) and continuous light stimulation (B). (C–F) Histogram plots of measurements performed on astrocytes in vitro. Data values corresponding to control standard extracellular solution are colored in gray, to G_q–PLC–IP_3 inhibitor U73122 in orange, and $G_{i/o}$ inhibitor PTX in purple. All the results are expressed as mean ± SEM and statistical *p*-values. (C) Maximal fluorescence variation, (D) percentage of responding cells, (E) time onset (first fluorescence variation above the cutoff of the baseline-0.1), and (F) time to first peak. Asterisks denote significant difference: *($p < 0.05$), ** ($p < 0.01$), *** ($p < 0.001$), **** ($p < 0.0001$). One-way ANOVA with Bonferroni correction. For $\Delta F/F$ (all cells, responding and not responding): ISF control $N = 101$, $n = 7$; ISF U73122 $N = 74$, $n = 3$; ISF PTX $N = 49$, $n = 3$; CL control $N = 129$, $n = 7$; CL U73122 $N = 36$, $n = 3$; CL PTX $N = 56$, $n = 3$. *N*, number of analyzed cells (regions of interest); *n*, number of experiments. Sample sizes vary by metric; *N* (cells/ROIs) and *n* (experiments) for each panel are reported in Tables S1–S5, and *p*-values in Tables S6–S10.

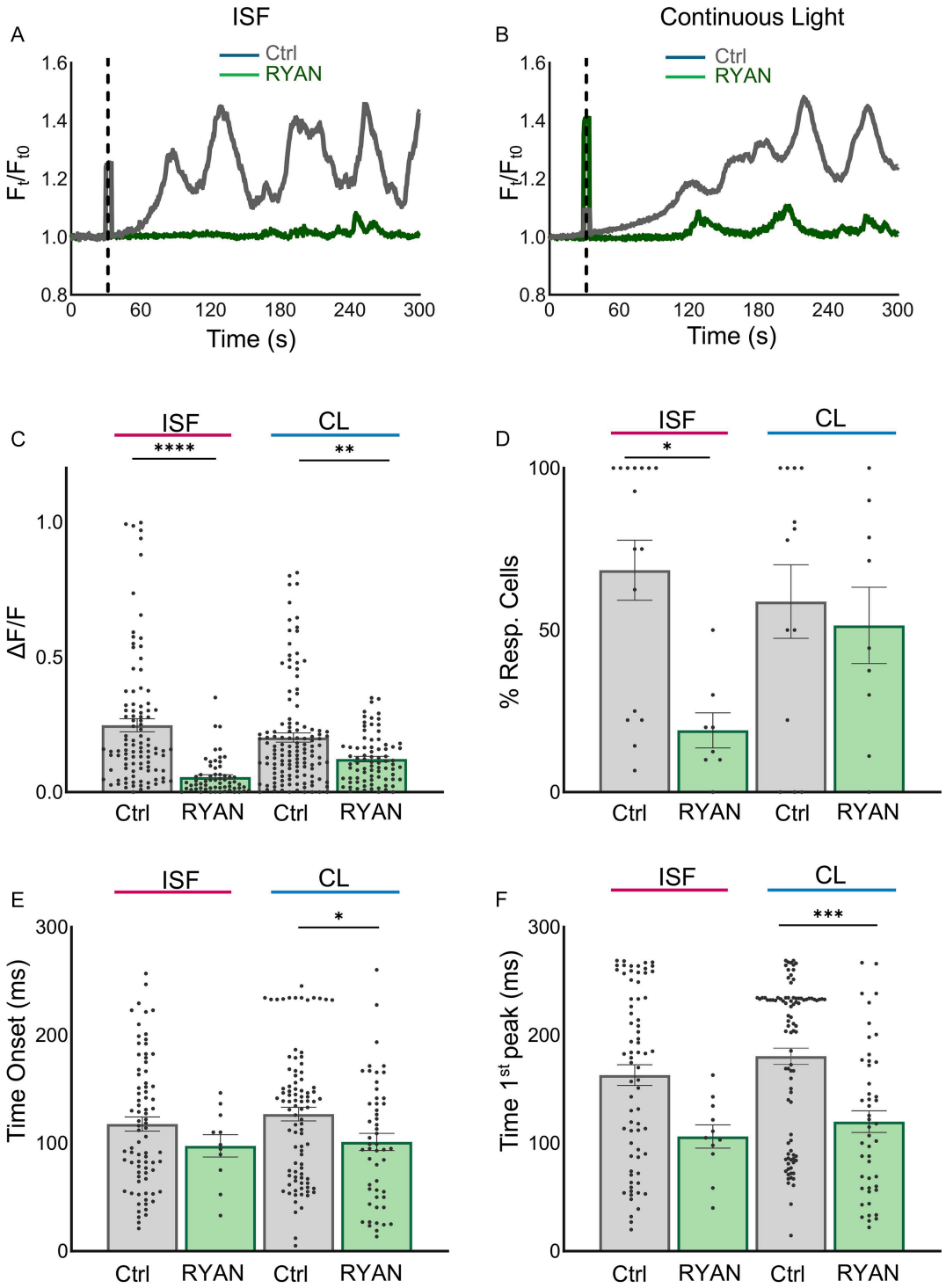

FIGURE 7 | Ryanodine receptor is involved in astrocytic responses after ISF and CL stimulation. (A,B) Representative traces of astrocyte calcium signaling using ryanodine receptor inhibitor ryanodine (RYR) (50 μM) after ISF (A) and continuous light stimulation (B). (C–F) Histogram plots of measurements performed on astrocytes in vitro. Data values corresponding to control standard extracellular solution are colored in gray and to RYAN in green. All the results are expressed as mean ± SEM and statistical *p*-values. (C) Maximal fluorescence variation, (D) percentage of responding cells, (E) time onset (first fluorescence variation above the cutoff of the baseline-0.1), and (F) time to first peak. Asterisks denote significant difference: *($p < 0.05$), **($p < 0.01$), ***($p < 0.001$), ****($p < 0.0001$), one-way ANOVA with Bonferroni correction. For $\Delta F/F$: ISF control $N = 101$, $n = 7$; ISF ryanodine $N = 55$, $n = 3$; CL control $N = 129$, $n = 7$; CL ryanodine $N = 81$, $n = 3$. *N*, number of analyzed cells (regions of interest); *n*, number of experiments. Sample sizes vary by metric; *N* (cells/ROIs) and *n* (experiments) for each panel are reported in Tables S1–S5, and *p*-values in Tables S6–S10.

to ~318 mOsm with mannitol. Ca^{2+}-free extracellular solution ($0[Ca^{2+}]_o$) was composed of (mM) 140 NaCl, 4 KCl, 4 MgCl2, 10 HEPES, 0.5 EGTA, pH 7.4 with NaOH, and osmolarity adjusted to ~318 mOsm with mannitol. Stock solution of 2-aminoethoxy diphenyl borate (2-APB, 100 mM) was prepared by dissolution in methanol and stored at −20°C. Stock solutions of RN-1734

(10 mM), HC-030031 (40 mM), and ryanodine (1.25 mM) were prepared by dissolution in dimethyl sulfoxide (DMSO) and stored at −20°C. GsMTx4 was prepared by dissolution in water and stored at −20°C. Stock solutions of PTX (7.5 µg mL^{-1}) were prepared by dissolving in distilled water and stored at 4°C. U-73122 hydrate stock solution (1.9 mM) was prepared by dissolution in DMSO and stored at −20°C. In experiments where astrocytes were stimulated while inhibiting G_q–PLC–IP_3 signaling, U-73122 was added to the standard bath solution. To inhibit $G_{i/o}$ signaling, cells were preincubated for 1 h in a standard solution containing the $G_{i/o}$ inhibitor PTX before the experiments.

2.6 | Data Analyses and Statistics

In calcium imaging experiments, the ratio of the fluorescence intensity at each time point and the initial fluorescence was continuously recorded during the experiment (Ft/Ft_0).

To evaluate the temporal features of calcium dynamics, we extracted the average number of peaks by detecting the number of fluorescence oscillations recorded over time, from the beginning of electrical stimulation until the end of the experiment (Figure S1). When a slow variation occurred, we quantified one peak on average. To characterize the diverse $[Ca^{2+}]_i$ temporal dynamics observed, we also estimated, for each cell, the average time to reach the maximal fluorescence increase after the voltage stimulus (time to peak).

The percentage of responding cells relative to the total number of cells observed is expressed as the percentage of responding cells (number of responding cells/number of total cells ×100).

The onset was calculated at the time point where we could measure the minimal variation (0.1 $\Delta F/F$) in $\Delta F/F$ after the photostimulation.

For in vitro experiments, somatic or process cellular fluorescence time series were manually extracted in both MetaFluor (Molecular Devices) and a dynamic-data-exchange Excel file (Microsoft Office 365). Representative traces and statistical analyses of extracted data from in vitro calcium imaging were then performed using Microcal Origin 8.5. Bar–dot plots were generated using Prism GraphPad 8.0.2. Data were compared using one-way ANOVA with Bonferroni post-test. A statistically significant difference was reported if $p \leq 0.05$. All data are presented as mean ± s.e.m. Sample size (n) for each statistical analysis is reported in the figure caption referring to the specific result. The data were analyzed from at least four independent experiments.

3 | Results

The goal of this study was to investigate the effect of ISF and CL light on astrocytic calcium dynamics. To this end, cortical primary astrocytes were plated on PDL-coated glass coverslips loaded with Fluo4-AM calcium fluorophore and imaged using an upright fluorescent microscope using an optical fiber positioned close to the cells, as shown in Figure 2A. Fluorescent images, which were sampled every 500 ms, collected before and after the stimulation with ISF and CL light, are reported in Figure 3A,B. Traces representative of typical somatic cell fluorescence variation over time (Ft/Ft_0) (Figure 3C,D), which correlates with changes in intracellular calcium concentration, show that both ISF and CL light elicit calcium responses in primary astrocytes (Figure 3).

The bar–dot plot in Figure 3E indicates that both ISF and CL stimulation produced a significant increase in maximal fluorescence variation, which corresponds to an increase in intracellular Ca^{2+} concentration compared to the basal (no-stimulation) condition. Notably, approximately 70% of the cells responded to ISF (68.48 ± 9.264), while nearly 60% (58.81 ± 11.36) activated calcium dynamics after CL (Figure 3F). The onset time of Ca^{2+} responses was comparable between ISF and CL stimulation (Figure 3G), whereas the time to the first fluorescence maximum (time to first peak) following ISF stimulation was significantly shorter (163 ± 9.553) than in the no-stimulation condition (202.4 ± 8.776) (Figure 3H). The dynamics were oscillatory both in response to ISF and CL, as shown by the analyses of number of peaks (Figure S1).

The possibility that the observed phenomena were attributable to a thermal effect of light stimulation was next evaluated. The temperature of the bath containing the cells was measured using a $NiCr^{-}/NiAl^{+}$ K-type thermocouple (RS) during ISF and CL stimulation for 10 min and was found to be stable (Table S11). Moreover, even under a conservative assumption of complete absorption of the delivered light, the expected temperature rise is negligible. The applied irradiance was 1.3 mW/cm^2 for 5 s, corresponding to a fluence of 6.5×10^{-3} J/cm^2. For a 35-mm-diameter Petri dish, area $A = \pi r^2 = \pi(1.75\ \text{cm})^2 \approx 9.62\ \text{cm}^2$. The total delivered energy is therefore $Q = (6.5 \times 10^{-3}\ \text{J/cm}^2) \times 9.62\ \text{cm}^2 \approx 6.25 \times 10^{-2}$ J. The corresponding *upper-bound* temperature increase is $\Delta T = Q/m\ c < 10^{-3}$ K, which for 2 mL of aqueous medium $m \approx 2$g, and $c = 4.186$ J/(g K) specific heat yields $\Delta T \approx 7.5 \times 10^{-3}$ K (≈7.5 mK), i.e., far below temperature changes known to influence astrocytic Ca^{2+} dynamics (typically >1°C–2°C). This estimate is conservative, as the fiber-coupled illumination geometry (2 cm distance, 45° incidence) disperses the beam and the effective illuminated area within the dish is likely smaller and/or nonuniform, reducing the actual absorbed energy.

The low excitation power also excludes the presence of localized heating sources (microheating). Under these conditions, the photon flux can be estimated as $\Phi \approx I/E_{\text{photon}}$. Assuming a mean wavelength of 550 nm, $E_{\text{photon}} = \frac{h_c}{\lambda} \approx 3.6 \times 10^{-19}$ J, giving $\Phi \approx (1.3 \times 10^{-3}\ \text{Js}^{-1}\text{cm}^{-2})/(3.6 \times 10^{-19}\ \text{J}) \approx 3.6 \times 10^{-15}$ photons s^{-1} cm^{-2}. In the absence of exogenous strong absorbers, light absorption is expected to be dominated by endogenous chromophores (e.g., in proteins, including at the cell membrane), with typical visible-light absorption cross-sections on the order of ~10^{-16} cm^2 [35]. This corresponds to an absorption rate per chromophore of $\Phi\sigma \approx 0.36\text{s}^{-1}$ (i.e., substantially less than one photon per second per chromophore). Given that excited-state relaxation occurs on subnanosecond timescales, absorbed energy would dissipate rapidly into the surrounding aqueous environment, arguing against the formation of physiologically meaningful localized micro-heating "hot spots" under the present stimulation conditions.

Pharmacological methods were employed to identify the underlying mechanisms of the observed Ca^{2+} rise after ISF and CL stimulation in control conditions. All results, presented as mean ± SEM along with statistical p-values, are detailed in the Supporting

Information. Substitution of standard saline solution (control) with external solution not containing Ca^{2+} ($0[Ca^{2+}]_o$) almost abolishes the Ca^{2+} response observed after stimulation with ISF (Figure 4). On the other hand, the response observed after CL was not significantly altered in its magnitude by removal of $[Ca^{2+}]_o$. Accordingly, the percentage of responding cells to ISF stimulation was almost nulled in the absence of external Ca^{2+}, while stimulation with CL evokes a Ca^{2+} response in a comparable number of cells as the one observed in standard saline (Figure 4D).

Under extracellular Ca^{2+} depletion ($0[Ca^{2+}]_o$), the time to the first peak was significantly shortened following CL stimulation compared with control conditions (Figure 4F).

Next, we applied 2-aminoethoxydiphenylborane (2-APB), an antagonist of inositol-3-phosphate receptors (IP_3R), at a concentration of 100 μM. Treatment with 2-APB led to significantly lower amplitude in the Ca^{2+} response after both ISF and CL stimulation compared to stimulation delivered in standard saline (Figure 4C). This effect was also accompanied by a decreased percentage of responding cells following both types of stimulation (Figure 4D).

These data indicate that extracellular Ca^{2+} influx largely mediates the astrocytic response to ISF and is required for the onset of the response, whereas Ca^{2+} signaling evoked by CL is largely independent of the presence of calcium ions in the extracellular solution. The results further indicate that IP_3R-mediated pathways play a crucial role in the calcium dynamics observed following ISF and CL stimulation. Notably, under Ca^{2+}-free conditions, the dynamics of CL evoked response still persist, but markedly change their shape, switching from a sustained profile to a more peaked response [36]. These data suggest that different stimulation frequencies, despite delivering the same total energy to the cells, may activate or recruit different calcium signaling pathways in astrocytes.

To get further insight on this hypothesis, we explored the effects of RN-1734 (10 μM), an antagonist of TRPV4 channels, and HC-030031 (40 μM), an antagonist of TRPA1 channels previously implicated in astrocytic responses to chemophysical stimuli [21, 36, 37]. RN-1734 significantly decreased the amplitude of the calcium signal evoked by ISF and CL (Figure 5C,D). In the case of the CL, the onset of the response and the time to the first peak were significantly shorter, and significantly more peaks in the low percentage of cells that responded (Figure 5E,F).

The addition of HC-030031 induced a significantly lower calcium response both after the stimulation with ISF and CL, accompanied by a slower onset of the responses compared to control conditions, as seen in Figure 5E. These data indicate that TRPV4 and TRPA1 contribute to the magnitude of the response observed after ISF and CL stimulation. However, while TRPV4 is essential for the onset of the response to ISF, it is not demanded for the activation of the calcium signaling in response to CL. On the other hand, TRPA1 is important for both ISF- and CL-induced effect to occur. The data is not surprising, as TRPA1 is known to regulate basal calcium signaling in astrocytes in vitro and *ex vivo* [14]. Thus, it is plausible that prolonged inhibition of TRPA1 hampers the possibility of the cell responding to the stimulation, as observed in previous studies [21]. TRPV4 can be activated by different types of stimuli, including agonists, changes in temperature, osmotic and volume imbalance, and mechanical stimulation [38, 39]. Previous studies indicated that infrared-light stimulation induces a thermo-mechanical effect, and osmotic effects that lead to Ca^{2+} signaling in astrocytes [21].

Given that we ruled out the possibility of a thermal effect, we hypothesized that a photomechanical response could be activated and that it could engage other mechanosensitive channels. To test this hypothesis, we explored the role of mechanosensitive ion channel Piezo-1 by applying GsMTx4, a peptide inhibitor of stretch-activated cationic mechanosensitive currents [40]. However, the addition of Piezo-1 inhibitor did not induce significant changes in response amplitude, percentage of responding cells, or kinetic parameters, for either ISF or CL stimulation. These data suggested that GsMTx4-sensitive mechanosensitive Ca^{2+}-influx did not make a major contribution to the observed Ca^{2+} effects, as seen in the Figure S1.

A recent study indicates that 40 HZ stimulation *in vivo* might impact on astrocytes' glymphatic system mediated by astrocytes, and suggested a mechanism that involves adenosine receptor activation, in primary astrocytes *in vitro* [32].

Adenosine receptors are a family of G-protein-coupled receptors (GPCR) that are known to mediate calcium signaling and neuroglial cell communication [41]. In addition, diverse GPCRs are differently engaged by astrocytes to respond to chemo-physical stimuli like electrical stimulation, ultrasound stimulation, and infrared light stimulation [36, 37].

To further investigate the underlying signaling mechanisms and the potential involvement of GPCRs in the observed behaviors, the effects of U73122 and pertussis toxin (PTX) were investigated. U73122, a phospholipase C (PLC) inhibitor, was used to assess the contribution of G_q–PLC-mediated IP_3 pathway. PLC inhibition with U73122 resulted in an increase in calcium signal amplitude after ISF stimulation (Figure 6C), while it had no significant effect on the magnitude of the response to CL. Interestingly, the time onset and time to first peak are faster with respect to those observed in the control saline solution (Figure 6E–F) after both ISF and CL stimulation. To block Gi/o signaling, cells were incubated in a standard solution containing the $G_{i/o}$ inhibitor PTX at a concentration of 500 ng ml^{-1}, for 1 h before conducting experiments. PTX treatment significantly increased the variation of fluorescence after CL stimulation but had no effect on ISF. Additionally, it significantly reduced both the onset time and the time to first peak exclusively following CL stimulation.

Several lines of evidence indicate that G_q and G_s have reciprocal effects in astrocytes [42–45]. The increase in signal amplitude observed in response to G_q inhibition, only after the stimulation with ISF, suggests that G_s signaling might become predominant and possibly mediate the response of astrocytes to ISF. Interestingly, G_q inhibition has no effect on CL magnitude, despite accelerating its onset. On the contrary, $G_{i/o}$ inhibition showed no effects on ISF stimulation, while severely altering the Ca^{2+} response to CL both in terms of magnitude and dynamics. All these data indicate that ISF and CL photostimulations engage different signaling pathways in astrocytes, possibly involving different GPCR metabotropic receptors.

As an additional intracellular signaling pathway, we explored the role of ryanodine receptors (RyRs) in the photostimulation-evoked responses to ISF and CL. *In vitro* studies have indicated that, in addition to IP_3Rs pathway, the release of Ca^{2+} from the endoplasmic reticulum can be triggered and amplified

by calcium-induced calcium release (CICR) mediated by Ca^{2+}-sensitive RyRs [46]. Accordingly, RyR-dependent CICR release was probed by applying ryanodine (50 μM) to functionally interfere with RyR-mediated ER Ca^{2+} release.

In the presence of RYR (50 μm), the amplitude ($\Delta F/F$) of the response to ISF was significantly reduced (Figure 7C) and the percentage of responding cells was significantly decreased (Figure 7D), whereas no significant differences were observed in time onset or time to first peak (Figure 7E,F, respectively). In the case of CL, the response amplitude ($\Delta F/F$) was also significantly reduced (Figure 7C), while the percentage of responding cells was not significantly changed; however, response kinetics were significantly faster, with a reduction in time onset (Figure 7E) and a shorter time to first peak (Figure 7F).

Notably, while inhibition of RyRs abolished the response to ISF in almost all the cells (Figure 7D), the same percentage of cells stimulated with CL still maintained a response that displayed an oscillatory behavior (Figure 7B). Indeed, ryanodine treatment was associated with significant changes in oscillatory structure, as reflected by the number of Ca^{2+} peaks, with a significant difference observed for ISF and a significant increase observed for continuous light (Table S10).

4 | Discussion

The key finding of this work is that ISF and continuous light stimulation (CL) elicit Ca^{2+} signaling responses in astrocytes. Interestingly, the pathways triggered by ISF and CL are distinct. Specifically, ISF stimulation needs both intracellular and extracellular Ca^{2+} sources to occur, whereas continuous light stimulation relies predominantly on intracellular Ca^{2+} mobilization to occur (Figures 3 and 4).

Notably, the sensitivity of astrocytes to photonic stimulation has previously been demonstrated using laser-based approaches [20–22]. The etiology of the observed phenomena is very unlikely to be attributable to thermal effects, as the delivered fluence was low (0.0065 J/cm^2) and no measurable temperature increase in the culture medium was detected. Importantly, irradiance and total fluence were matched between ISF and continuous light conditions; thus, the sole distinguishing feature of ISF relative to continuous stimulation was the presence of a 40 Hz invisible spectral alternation.

Under low-fluence visible light in the absence of classical photoreceptors, photon absorption is plausibly mediated by endogenous chromophores—most prominently mitochondrial redox components such as cytochrome c oxidase and flavoproteins, leading to downstream changes in mitochondrial redox/ROS and cellular signaling that can couple to Ca^{2+} dynamics [24, 47–49].

The differing effects of RN-1734 and HC-030031 on response magnitude and kinetics indicate that TRPV4 and TRPA1 contribute to light-evoked Ca^{2+} responses under both ISF and continuous stimulation. In a previous study, IP_3 signaling and TRPV4/TRPA1 involvement were reported in the mechanisms underlying water and Ca^{2+} dynamics in astrocytes stimulated with pulsed infrared light [21]. The engagement of these channels by visible LED light is of interest, as the present stimulation did not measurably increase temperature, did not require laser illumination, and avoids certain pitfalls of other stimulation modalities. In the present framework, TRPA1/TRPV4-dependent Ca^{2+} entry is proposed to provide an initiating and/or permissive Ca^{2+} signal coupling membrane-level events to ER Ca^{2+} mobilization via IP_3R and RyR-dependent amplification [21, 50].

Since recruitment of IP_3R-dependent ER release is frequently driven by GPCR signaling, the involvement of GPCR-mediated pathways was investigated. The results indicated that astrocytes recruit distinct downstream signaling components in response to ISF versus CL stimulation, as supported by differential sensitivity to U73122 and PTX, consistent with regulation by G-protein signaling. It is worth noting that $G_{i/o}$ inhibition affects CL but not ISF.

Recent *in vivo* work [32] has identified adenosine signaling as a key mediator of 40 Hz light flicker effects on glymphatic function, based on increased cerebrospinal adenosine levels and the abolishment of the flicker-induced glymphatic enhancement following genetic or pharmacological inactivation of ENT2 or A_2A receptors (A_2ARs), together with evidence for physical and functional A_2AR–AQP4 interaction in astrocytes *in vitro* [32]. Previous studies support the functional and molecular interaction of AQP4 with the intracellular calcium signaling of astrocytes, also mediated by TRPV4 [11, 51, 52]. Thus, we might envisage that, given the observed role of TRPV4 in the calcium signaling elicited by both ISF and CL, AQP4 and or water permeability might be influenced by LED light stimulation. Future studies will clarify this aspect. The strong dependence of light-evoked Ca^{2+} signals on ER release mechanisms (2-APB sensitivity) and modulation by GPCR pathway inhibitors, together with stimulation-dependent regulation by RyR-dependent CICR, is compatible with the possibility that purinergic/adenosinergic signaling acts as a modulatory layer that shapes astrocytic Ca^{2+} gain and downstream outputs.

Overall, the present results demonstrate that astrocytes can discriminate between distinct forms of noncoherent visible photonic stimulation and engage different Ca^{2+} signaling pathways in response. This provides a foundation for manipulating astrocytic Ca^{2+} dynamics using a simple, label-free optical approach, without reliance on opto- or chemogenetic tools. The present work specifically establishes an experimental platform for investigating the effects of 40 Hz invisible spectral flicker light on Ca^{2+} dynamics in primary astrocytes *in vitro*.

ISF has been investigated as a noninvasive approach to elicit gamma oscillations in healthy controls [29, 53], as well as a therapeutic approach in Alzheimer's disease [54, 55] and major depressive disorder [56]. While the underlying mechanisms of potential therapeutic effects remain incompletely understood, preclinical and early clinical work has suggested protective effects of gamma entrainment on neurons and glial cells, including microglia [57–60].

It is emphasized that the present study does not aim to provide a mechanistic explanation of the *in vivo* effects of ISF, as brain-level effects are indirect, and the pathways involved are not necessarily equivalent across cell types or experimental contexts. However, the identification of light-responsive Ca^{2+}

pathways in astrocytes calls for further investigation of astrocytic contributions to stimulation paradigms used to drive gamma-range activity.

In this context, it is worth noting the molecular and functional similarity between astrocytes and other glial cell types closely associated with light-sensitive tissues, such as Müller glia in the retina. Müller glia and retinal ganglion neurons express key components of Ca^{2+} signaling, including TRPV4, TRPA1, and IP_3 receptors, suggesting the possibility that shared channel and store-release architectures may support light-responsive Ca^{2+} dynamics across glial systems [61].

In the broader context, gamma light stimulation has emerged as a promising modulator of glymphatic clearance, a process implicated in neurodegenerative diseases [33]. Given evidence that neuro and gliotransmitters such as adenosine can enhance glymphatic transport via AQP4-dependent mechanisms, targeted optical stimulation may offer a strategy to modulate brain waste clearance in a controlled manner [32]. Considering the partnership of AQP4 with calcium channels and signaling ex vivo in astrocytes [11, 62], but also in Müller glia [63, 64], an impact of 40 Hz light on calcium signaling in cells of visual sensory organs would be plausible. However, whether a calcium signaling component can be activated in optical sensory cells by 40 Hz light remains to be elucidated.

In summary, the present study contributes to a growing field of gliophotonics [19] by demonstrating that visible LED light delivered with matched fluence but distinct temporal-spectral structure can engage distinct astrocytic Ca^{2+} pathways. While further work is required to resolve upstream transduction mechanisms and to establish how astrocytic responses interface with neuronal circuitry and *in vivo* physiology, these findings provide a basis for developing new tools to probe astrocyte function in health and disease.

Author Contributions

V.B. conceived the concept, designed the experiments, interpreted the results, discussed the mechanism, revised the manuscript, and coordinated the work. A.K. performed the calcium microfluometry experiments, analyzed and discussed the results, set up the experimental design, and wrote the manuscript. M.H. built the device, set up the experimental design, and wrote the manuscript. T.E.R. built the device. M.S.C. conceived and discussed the concept. A.C. performed the temperature acquisition calculations and discussed the results. A.K., R.F., C.L., G.C., and M.C. prepared and maintained the primary rat astrocytic cultures.

Acknowledgments

This project is funded by the European Union's Horizon 2020 research and innovation program under the Marie Skłodowska–Curie grant agreement 956325 (ASTROTECH). A.K. and M.H. are financed by ASTROTECH. R.F. is supported by the Air Force Office of Scientific Research ASTROTALK FA9550–23–1–0736 and ASTROSENSE FA9550-25-01-0001. M.S.C. has partial ownership of OptoCeutics ApS. We thank Gustavo Miguel Feijóo from OC for his advice and expertise in the device design. We thank Andrea Barbieri for his advice and technical support while setting up the experimental apparatus and thermal measurements.

Open access publishing facilitated by Consiglio Nazionale delle Ricerche, as part of the Wiley - CRUI-CARE agreement.

Funding

This work was supported by the H2020 Marie Skłodowska-Curie Actions (956325-ASTROTECH), Air Force Office of Scientific Research (FA9550-25-1-0001, FA9550-23-1-0736).

Conflicts of Interest

The authors declare no conflicts of interest.

Data Availability Statement

The data that support the findings of this study are available from the corresponding author upon reasonable request.

References

1. E. Hansson and L. Rönnbäck, "Glial Neuronal Signaling in the Central Nervous System," *FASEB Journal* 17 (2003): 341–348.

2. W. S. Chung, N. J. Allen, and C. Eroglu, "Astrocytes Control Synapse Formation, Function, and Elimination," *Cold Spring Harbor Perspectives in Biology* 7 (2015): a020370.

3. A. Konstantoulaki, R. Fabbri, G. Conte, C. Lazzarini, and V. Benfenati, "Astrocytes Multiscale Molecular Targets for Glial Engineering and Interfaces," in Glial Engineering and Glial Interfaces: Targeting the Role of Astrocytes and Other Glial Cells in Brain Function and Dysfunctions, (Springer Nature, 2025), 1-46, https://doi.org/10.1007/978-3-031-94215-0_1/FIGURES/1.

4. R. C. Koehler, D. Gebremedhin, and D. R. Harder, "Role of Astrocytes in Cerebrovascular Regulation," *Journal of Applied Physiology (1985)* 100 (2006): 307–317.

5. M. Simard and M. Nedergaard, "The Neurobiology of Glia in the Context of Water and Ion Homeostasis," *Neuroscience* 129 (2004): 877–896.

6. J. F. Oliveira and A. Araque, "Astrocyte Regulation of Neural Circuit Activity and Network States," *Glia* 70 (2022): 1455–1466.

7. Y. Buskila, A. Bellot-Saez, and J. W. Morley, "Generating Brain Waves The Power of Astrocytes," *Frontiers in Neuroscience* 13 (2019): 488323.

8. J. Lines, E. D. Martin, P. Kofuji, J. Aguilar, and A. Araque, "Astrocytes Modulate Sensory-Evoked Neuronal Network Activity," *Nature Communications* 11 (2020): 1–12.

9. R. D. Fields, D. H. Woo, and P. J. Basser, "Glial Regulation of the Neuronal Connectome through Local and Long-Distant Communication," *Neuron* 86 (2015): 374–386.

10. N. Bazargani and D. Attwell, "Astrocyte Calcium Signaling: The Third Wave," *Nature Neuroscience* 19 (2016): 182–189.

11. V. Benfenati, M. Caprini, M. Dovizio, et al., "An Aquaporin-4/Transient Receptor Potential Vanilloid 4 (AQP4/TRPV4) Complex Is Essential for Cell-Volume Control in Astrocytes," *Proceedings of the National Academy of Sciences of the United States of America* 108 (2011): 2563–2568.

12. V. Benfenati, M. Amiry-Moghaddam, M. Caprini, et al., "Expression and Functional Characterization of Transient Receptor Potential Vanilloid-Related Channel 4 (TRPV4) in Rat Cortical Astrocytes," *Neuroscience* 148 (2007): 876–892.

13. E. Shigetomi, X. Tong, K. Y. Kwan, D. P. Corey, and B. S. Khakh, "TRPA1 Channels Regulate Astrocyte Resting Calcium Levels and Inhibitory Synapse Efficacy via GAT-3," *Nature Neuroscience* 15 (2012): 70.

14. E. Shigetomi, O. Jackson-Weaver, R. T. Huckstepp, T. J. O'Dell, and B. S. Khakh, "TRPA1 Channels Are Regulators of Astrocyte Basal Calcium

Levels and Long-Term Potentiation via Constitutive d-Serine Release," *Journal of Neuroscience* 33 (2013): 10143–10153.

15. M. J. Berridge, M. D. Bootman, and H. L. Roderick, "Calcium Signalling: Dynamics, Homeostasis and Remodelling," *Nature Reviews Molecular Cell Biology* 4 (2003), https://doi.org/10.1038/nrm1155

16. G. Di Benedetto, C. Burgaletto, C. M. Bellanca, A. Munafò, R, Bernardini, and G. Cantarella, "Role of Microglia and Astrocytes in Alzheimer's Disease: From Neuroinflammation to Ca2+ Homeostasis Dysregulation," *Cells* 11 (2022): 2728.

17. P. J. Magistretti, "Neuron-Glia Metabolic Coupling and Plasticity," *Journal of Experimental Biology* 209 (2006): 2304–2311.

18. A. L. Naour, E. Beziat, J. H. Kam, P. Magistretti, A.-L. Benabid, and J. Mitrofanis, "Do Astrocytes Respond to Light, Sound, or Electrical Stimulation?," *Neural Regeneration Research* 18 (2023): 2343–2347.

19. L. Maiolo, V. Guarino, E. Saracino, et al., "Glial Interfaces: Advanced Materials and Devices to Uncover the Role of Astroglial Cells in Brain Function and Dysfunction," *Advanced Healthcare Materials* 10, no. 1 (2021): 2001268.

20. X. Lv, Y. Zhang, X. Liu, et al., "Photostimulation of Astrocytes with Femtosecond Laser Pulses," *Optics Express* 17, no. 3 (2009): 1291–1298.

21. A. I. Borrachero-Conejo, W. R. Adams, E. Saracino, et al., "Stimulation of Water and Calcium Dynamics in Astrocytes with Pulsed Infrared Light," *FASEB Journal* 34 (2020): 6539–6553.

22. D. Spennato, J. Leone, C. Gundhardt, et al., "Investigations of Astrocyte Calcium Signaling and Imaging with Classical and Nonclassical Light," *Journal of Physical Chemistry B* 128 (2024): 7966–7977.

23. B. J. Raos, E. S. Graham, and C. P. Unsworth, "Nanosecond UV Lasers Stimulate Transient Ca2+ Elevations in Human hNT Astrocytes," *Journal of Neural Engineering* 14 (2017): 035001.

24. M.-J. Jou, S.-B. Jou, M.-J. Guo, H.-Y. Wu, and T.-I. Peng, "Mitochondrial Reactive Oxygen Species Generation and Calcium Increase Induced by Visible Light in Astrocytes," *Annals of the New York Academy of Sciences* 2004 (1011): 45–56.

25. C. Vicente-Gutierrez, Nó Bonora, V. Bobo-Jimenez, et al., "Astrocytic Mitochondrial ROS Modulate Brain Metabolism and Mouse Behaviour," *Nature Metabolism* 1 (2019): 201–211.

26. E. Stuntz, Y. Gong, D. Sood, et al., "Endogenous Two-Photon Excited Fluorescence Imaging Characterizes Neuron and Astrocyte Metabolic Responses to Manganese Toxicity," *Scientific Reports* 7 (2017): 1041.

27. J. Hoh Kam, R. Clément, T. Cantat-Moltrecht, M. Billères, and J. Mitrofanis, "Red and Near-Infrared Light Treatment Can Change the Intensity of Biophoton Emissions in Cell Culture," *Scientific Reports* 15 (2025): 38541.

28. M. S. Carstensen, J. Lindén, N. M. Nguyen, et al., "*40 Hz Invisible Spectral Flicker and Its Potential use in Alzheimer's Light Therapy Treatment*" 11221 (2020): 47–58, https://doi.org/10.1117/12.2544338.

29. L. S. Hansen, M. H. Carstensen, M. A. Henney, et al., "Light-Based Gamma Entrainment with Novel Invisible Spectral Flicker Stimuli," *Scientific Reports* 14 (2024): 1–17.

30. A. C. Singer, A. J. Martorell, J. M. Douglas, et al., "Noninvasive 40-Hz Light Flicker to Recruit Microglia and Reduce Amyloid Beta Load," *Nature Protocols* 13 (2018): 1850–1868.

31. T. Tian, X. Qin, Y. Wang, Y. Shi, and X. Yang, "Hz Light Flicker Promotes Learning and Memory via Long Term Depression in Wild-Type Mice," *Journal of Alzheimer's Disease* 84 (2021): 983–993.

32. X. Sun, L. Dias, C. Peng, et al., "40 Hz Light Flickering Facilitates the Glymphatic Flow via Adenosine Signaling in Mice," *Cell Discovery* 10 (2024): 81.

33. M. H. Murdock, C.-Y. Yang, N. Sun, et al., "Multisensory Gamma Stimulation Promotes Glymphatic Clearance of Amyloid," *Nature* 627 (2024): 149–156.

34. S. Ferroni, C. Marchini, P. Schubert, and C. Rapisarda, "Two Distinct Inwardly Rectifying Conductances Are Expressed in Long Term Dibutyryl-Cyclic-AMP Treated Rat Cultured Cortical Astrocytes," *Febs Letters* 367 (1995): 319–325.

35. M. Taniguchi and J. S. Lindsey, "Database of Absorption and Fluorescence Spectra of >300 Common Compounds for use in PhotochemCAD," *Photochemistry and Photobiology* 94 (2018): 290–327.

36. R. Fabbri, et al., "Graphene Oxide Electrodes Enable Electrical Stimulation of Distinct Calcium Signalling in Brain Astrocytes," *Nature Nanotechnology* 19 (2024): 1–1353, https://doi.org/10.1038/s41565-024-01711-4.

37. W. R. Adams, A.I. Borrachero-Conejo, P. K. Rasiah, et al., "Infrared Neural Stimulation Elicits Distinct Molecular Pathways in Astrocytes Based on Laser Pulse Parameters," *Advances in Biology* 9 (2025): e00269.

38. B. Nilius, J. Vriens, J. Prenen, G. Droogmans, and T. Voets, "TRPV4 Calcium Entry Channel: A Paradigm for Gating Diversity," *American Journal of Physiology-Cell Physiology* 286 (2004): C195-C205, https://doi.org/10.1152/ajpcell.00365.2003.

39. F. Vincent and M. A. J. Duncton, "TRPV4 Agonists and Antagonists," *Current Topics in Medicinal Chemistry* 11 (2011): 2216–2226.

40. R. Gnanasambandam, C. Ghatak, A. Yasmann, et al., "GsMTx4: Mechanism of Inhibiting Mechanosensitive Ion Channels," *Biophysical Journal* 112 (2017): 31.

41. P. Kofuji and A. Araque, "G-Protein-Coupled Receptors in Astrocyte–Neuron Communication," *Neuroscience* 456 (2021): 71–84.

42. E. Hansson, P. Simonsson, and C. Alling, "Interactions between Cyclic AMP and Inositol Phosphate Transduction Systems in Astrocytes in Primary Culture," *Neuropharmacology* 29 (1990): 591–598.

43. A. Horvat, R. Zorec, and N. Vardjan, "Adrenergic Stimulation of Single Rat Astrocytes Results in Distinct Temporal Changes in Intracellular Ca2+ and cAMP-Dependent PKA Responses," *Cell Calcium* 59 (2016): 156–163.

44. M. Sobolczyk and T. Boczek, "Astrocytic Calcium and cAMP in Neurodegenerative Diseases," *Frontiers in Cellular Neuroscience* 16 (2022): 889939.

45. J. I. E. Bruce, S. V. Straub, and D. I. Yule, "Crosstalk between cAMP and CA2+ Signaling in Non-Excitable Cells," *Cell Calcium* 34 (2003): 431–444.

46. U. Lalo and Y. Pankratov, "Astrocyte Ryanodine Receptors Facilitate Gliotransmission and Astroglial Modulation of Synaptic Plasticity," *Frontiers in Cellular Neuroscience* 18 (2024): 1382010.

47. K. D. Desmet, D. A. Paz, J. J. Corry, et al., "Clinical and Experimental Applications of NIR-LED Photobiomodulation," *Photomedicine and Laser Surgery* 24 (2006): 121–128.

48. M. T. T. Wong-Riley, H. L. Liang, J. T. Eells, et al., "Photobiomodulation Directly Benefits Primary Neurons Functionally Inactivated by Toxins: Role of Cytochrome c Oxidase," *Journal of Biological Chemistry* 280 (2005): 4761–4771.

49. T. Karu, "Primary and Secondary Mechanisms of Action of Visible to Near-IR Radiation on Cells," *Journal of Photochemistry and Photobiology. B, Biology* 49 (1999): 1–17.

50. J. Strzelecka, D. W. Mazurkiewicz, T. Skadorwa, J. S. Gąsior, and S. Jóźwiak, "Photo-Dependent Reflex Seizures—A Scoping Review with Proposal of Classification," *Journal of Clinical Medicine* 11, no. 13 (2022): 3766.

51. M. G. Mola, A. Sparaneo, C. D. Gargano, et al., "The Speed of Swelling Kinetics Modulates Cell Volume Regulation and Calcium Signaling in Astrocytes: A Different Point of View on the Role of Aquaporins," *Glia* 64 (2016): 139–154.

52. B. Barile, M. G. Mola, F. Formaggio, et al., "AQP4-Independent TRPV4 Modulation of Plasma Membrane Water Permeability," *Frontiers in Cellular Neuroscience* 17 (2023): 1247761.

53. M. P. Agger, M. S. Carstensen, M. A. Henney, et al., "Novel Invisible Spectral Flicker Induces 40 Hz Neural Entrainment with Similar Spatial Distribution as 40 Hz Stroboscopic Light," *Journal of Alzheimer's Disease* 88 (2022): 335–344.

54. M. P. Agger, M. Horning, M. S. Carstensen, et al., "Study on the Effect of 40 Hz Non-Invasive Light Therapy System. A Protocol for a Randomized, Double-Blinded, Placebo-Controlled Clinical Trial," *Frontiers in Aging Neuroscience* 15 (2023): 1250626.

55. M. P. Agger, E. R.æk Danielsen, M. S. Carstensen, et al., "Safety, Feasibility, and Potential Clinical Efficacy of 40 Hz Invisible Spectral Flicker versus Placebo in Patients with Mild-to-Moderate Alzheimer's Disease: A Randomized, Placebo-Controlled, Double-Blinded Pilot Study," *Journal of Alzheimer's Disease* 92 (2023): 653–665.

56. L. Sakalauskaitė, L. S. Hansen, J. M. Dubois, et al., "Rationale and Design of a Double-Blinded, Randomized Placebo-Controlled Trial of 40 Hz Light Neurostimulation Therapy for Depression (FELIX)," *Annals of Medicine* 56 (2024): 2354852.

57. C. Adaikkan and L. H. Tsai, "Gamma Entrainment Impact on Neurocircuits, Glia, and Therapeutic Opportunities," *Trends in Neurosciences* 43 (2020): 24–41.

58. A. Guan, S. Wang, A. Huang, et al., "The Role of Gamma Oscillations in Central Nervous System Diseases: Mechanism and Treatment," *Frontiers in Cellular Neuroscience* 16 (2022): 962957.

59. C. Blanco-Duque, D. Chan, M. C. Kahn, M. H. Murdock, and L. H. Tsai, "Audiovisual Gamma Stimulation for the Treatment of Neurodegeneration," *Journal of Internal Medicine* 295 (2024): 146–170.

60. M. Horning and N. Aasheim, "Novel Treatment Options Through Light-Based Neurostimulation.," in Glial Engineering and Glial Interfaces: Targeting the Role of Astrocytes and Other Glial Cells in Brain Function and Dysfunctions, (Springer Nature, 2025), 151–199, https://doi.org/10.1007/978-3-031-94215-0_6/FIGURES/3.

61. Y. Wang, W. Zhang, G. Xu, et al., "The Role of TRPV4 in the Regulation of Retinal Ganglion Cells Apoptosis in Rat and Mouse," *Heliyon* 9 (2023): e17583.

62. A. S. Thrane, P. M. Rappold, T. Fujita, et al., "Critical Role of Aquaporin-4 (AQP4) in Astrocytic Ca2+ Signaling Events Elicited by Cerebral Edema," *Proceedings of the National Academy of Sciences of the United States of America* 108 (2011): 846–851.

63. A. O. Jo, D. A. Ryskamp, T. T. T. Phuong, et al., "TRPV4 and AQP4 Channels Synergistically Regulate Cell Volume and Calcium Homeostasis in Retinal Müller Glia," *Journal of Neuroscience* 35 (2015): 13525–13537.

64. A. Iuso and D. Križaj, "TRPV4-AQP4 Interactions 'Turbocharge' Astroglial Sensitivity to Small Osmotic Gradients," *Channels* 10 (2016): 172.

Supporting Information

Additional supporting information can be found online in the Supporting Information section. **Supporting Fig. S1: Histograms of the number of Ca^{2+} transient peaks per cell measured by calcium imaging in in-vitro astrocytes following ISF or continuous-light stimulation. Distributions are shown for each condition; summary values are reported as mean ± SEM. A)** Data values corresponding to ISF in control conditions and CL in control conditions are colored in magenta and dark blue respectively. Asterisks denote significant difference: * ($p<0.05$), ** ($p<0.01$), *** ($p<0.001$), **** ($p<0.0001$), One-way ANOVA with Bonferroni Correction. ISF N=82, n=7; CL N=88, n=7 **B)** Data values corresponding to control are colored in gray, $0[Ca^{2+}]_o$ in red, and 2-APB in blue. ISF control N=82, n=7; ISF $0[Ca^{2+}]_o$ N=23, n=5; ISF 2-APB N=3, n=4; CL control N=88, n=7; CL $0[Ca^{2+}]_o$ N=48, n=5; CL 2-APB N=11, n=4 **C)** Data values corresponding to control are colored in gray, to RN-1734 (RN) in teal and HC-030031 (HC) in gold. ISF control N=82, n=7; ISF RN-1734 N=18, n=4; ISF HC-030031 N=10, n=3; CL control N=88, n=7; CL RN-1734 N=8, n=4; CL HC-030031 N=8, n=3. **D)** Data values corresponding to control standard extracellular solution are colored in gray, to G_q–PLC–IP_3 inhibitor U73122 in orange, and $G_{i/o}$ inhibitor PTX in purple. **E)** Data values corresponding to the control standard extracellular solution are colored in gray, and to RYAN in green. ISF control N=82, n=7; ISF ryanodine N=14, n=3; CL control N=88, n=7; CL ryanodine N=42, n=3. **F)** Data values corresponding to the control standard extracellular solution are colored in gray, and those for MSCs inhibitor GsMTx4 (1 μM) are colored in pink. ISF control N=82, n=7; ISF GsMTx4 N=56, n=3; CL control N=88, n=7; CL GsMTx4 N=50, n=3. *N*, number of peaks per cell/ROI, and *n*, number of experiments for each panel, are reported in Tables S1–S5, and p-values in Tables S6–S10. **Supporting Fig. S2: Involvement of cationic mechanosensitive ion channels (MSCs) in astrocytic responses after ISF and Continuous Light stimulation. A-D)** Histogram plots of measurements performed on astrocytes *in vitro* after ISF and continuous light stimulation. Data values corresponding to the control standard extracellular solution are colored in gray, and those for MSCs inhibitor GsMTx4 (1 μM) are colored in pink. All the results are expressed as mean ± SEM and statistical p-values. **A)** Maximal fluorescence variation, **B)** percentage of responding cells, **C)** Time onset (first fluorescence variation above the cut-off of the baseline-0.1), **D)** Time to first peak. For ΔF/F (all cells, responding and not responding): ISF control N=101, n=7; ISF GsMTx4 N=78, n=3; CL control N=129, n=7; CL GsMTx4 N=81, n=3. *N*, number of analyzed cells (regions of interest), *n*, number of experiments. Sample sizes vary by metric; N (cells/ROIs) and n (experiments) for each panel are reported in Tables S1–S5, and p-values in Tables S6–S10. **Supporting Table S1**: Data values of means of maximal fluorescence variation (ΔF/F), ± Standard Error of the Mean (SEM), N=number of cells, n=number of experiments reported in Figures 3-7 and Figure S 1. **Supporting Table S2**: Data values of means of percentage of responding cells (% Resp Cells) ± Standard Error of the Mean (SEM), N=number of cells, n=number of experiments reported in Figures 3–7 and Figure S 1. **Supporting Table S3**: Data values of means of Time Onset (ms) ± Standard Error of the Mean (SEM), N=number of cells, n=number of experiments reported in Figures 3–7 and Figure S 1.**Supporting Table S4**: Data values of means of Time to first Peak (ms) ± Standard Error of the Mean (SEM), N=number of cells, n=number of experiments reported in Figures 3–7 and Figure S 1. **Supporting Table S5**: Data values of means of Number of Peaks ± Standard Error of the Mean (SEM), N=number of cells, n=number of experiments reported in Figures 3–7 and Figure S 1. **Supporting Table S6**: Data values referred to the histogram plots in Figures 3–7 and Figure S 1, regarding maximal fluorescence variation (ΔF/F). Here are reported the means difference between different conditions, the statistical significance and the p–values. One–way ANOVA was performed with Bonferroni's test for means comparisons. **Supporting Table S7**: Data values referred to the histogram plots in Figures 3–7 and Figure S 1, regarding the percentage of responding cells. Here are reported the means difference between different conditions, the statistical significance and the p–values. One–way ANOVA was performed with Bonferroni's test for means comparisons. **Supporting Table S8**: Data values referred to the histogram plots in Figures 3–7 and Figure S 1, regarding the time onset. Here are reported the means difference between different conditions, the statistical significance and the p–values. One–way ANOVA was performed with Bonferroni's test for means comparisons. **Supporting Table S9**: Data values referred to the histogram plots in Figures 3–7 and Figure S 1, regarding the time to the first peak. Here are reported the means difference between different conditions, the statistical significance and the p–values. One–way ANOVA was performed with Bonferroni's test for means comparisons. **Supporting Table S10**: Data values referred to the histogram plots in Figures 3–7 and Figure S 1, regarding the number of peaks. Here are reported the means difference between different conditions, the statistical significance and the p–values. One–way ANOVA was performed with Bonferroni's test for means comparisons. **Supporting Table S11: Temperature measurements of** the cell bath contained in a petri dish measured with a $NiCr^-/NiAl^+$ K–type thermocouple (RS) for 10 min of ISF, and CL stimulation.